

Galactic Orbits of Hipparcos Stars: Classification of Stars

G. A. Gontcharov and A. T. Bajkova

Pulkovo Astronomical Observatory, Russian Academy of Sciences, St.-Petersburg, Russia

Abstract—The Galactic orbits of 27 440 stars of all classes with accurate coordinates and parallaxes of more than 3 mas from the Hipparcos catalogue, proper motions from the Tycho-2 catalogue, and radial velocities from the Pulkovo Compilation of Radial Velocities (PCRV) are analyzed. The sample obtained is much more representative than the Geneva–Copenhagen survey and other studies of Galactic orbits in the solar neighborhood. An estimation of the influence of systematic errors in the velocities on orbital parameters shows that the errors of the proper motions due to the duplicity of stars are tangible only in the statistics of orbital parameters for very small samples, while the errors of the radial velocities are noticeable in the statistics of orbital parameters for halo stars. Therefore, previous studies of halo orbits may be erroneous. The distribution of stars in selection-free regions of the multidimensional space of orbital parameters, dereddened colors, and absolute magnitudes is considered. Owing to the large number of stars and the high accuracy of PCRV radial velocities, nonuniformities of this distribution (apart from the well-known dynamical streams) have been found. Stars with their peri- and apogalacticons in the disk, perigalacticons in the bulge and apogalacticons in the disk, perigalacticons in the bulge and apogalacticons in the halo, and perigalacticons in the disk and apogalacticons in the halo have been identified. Thus, the bulge and the halo are inhomogeneous structures, each consisting of at least two populations. The radius of the bulge has been determined: 2 kpc.

1 INTRODUCTION

Using the stellar coordinates α and δ , parallaxes π from the Hipparcos catalogue (van Leeuwen 2007), proper motions μ from the Tycho-2 catalogue (Hög et al. 2000), and radial velocities V_r allows not only the complete set of coordinates X , Y , Z and velocity components U , V , W , but also the Galactic orbits of stars to be calculated.

Because of the small number of stars with accurate V_r and because of the distrust in the joint use of μ and V_r , the Galactic orbits have been investigated so far only for small lists of stars, as a rule, obtained with the same instrument. Since the samples are incomplete, the studies of the orbits for stars that do not belong to the Galactic disk are particularly poor.

The appearance of the Pulkovo Compilation of Radial Velocities for 35 493 Hipparcos stars (PCRV; Gontcharov 2006), in which the systematic errors of V_r were taken into account and all the main classes of stars are represented, allows one to set the task of comprehensively studying the statistical characteristics of samples of stars based on their Galactic orbits by invoking their metallicities and ages.

The PCRV is still the largest source of V_r with included systematic errors. The median accuracy of V_r from the PCRV is 0.7 km s.⁻¹; V_r is more accurate than 5 km s.⁻¹ for all stars. The PCRV includes the values of V_r from 203 catalogues for which the systematic errors

detected in them were taken into account. These include the two largest present-day catalogues: the Geneva–Copenhagen survey (GCS) of more than 14 000 stars mostly of types FV–GV near the Sun (Nordström et al. 2004; Holmberg et al. 2007, 2009) and the kinematic survey of more than 6000 KIII–MIII stars based on CORAVEL observations (Famaey et al. 2005). The velocity components and Galactic orbits for 11 218 stars calculated in the GCS are used in this study to check the results, while the metallicities Fe/H for 11 615 stars and the ages for 10 249 stars calculated in the GCS will be used in our subsequent studies of the age–kinematics and metallicity–kinematics relations for various groups of stars.

2 DATA REDUCTION

The sample considered below is limited in parallax, $\pi > 3$ milliarcseconds (mas), for the following reasons. No firm conclusions can be reached about regions far from the Sun, where the PCRV includes few stars, while the limitation $\pi < 3$, leaving most of the stars in the sample (28 600, 80.6%), corresponds to a space where the PCRV is sufficiently representative. In addition, the accuracy of the components $\mu_\alpha \cos \delta$ and μ_δ for the overwhelming majority of PCRV stars is higher than 3 mas yr^{-1} . This value corresponds to the accuracy of V_r used (higher than 5 km s^{-1}) at a distance of 333 pc. The limitation of the sample at this distance makes it homogeneous with regard to the accuracy of the velocity components U , V , W . It is also important that, according to our numerical simulations (see Gontcharov 2012a), the Lutz–Kelker and Malmquist biases are negligible under the mentioned limitation in π . These are the biases of the sample’s statistical characteristics, primarily the distances and absolute magnitudes of the stars being determined, that arise when the sample is limited in measured parallax and/or in observed magnitude (Perryman 2009, pp. 208–212).

In addition to $\pi > 3$ mas, we adopted the following limitations: the relative accuracy is $\sigma(\pi)/\pi < 0.5$ (59 stars were lost), the accuracies of the components are $\sigma(\mu_\alpha \cos \delta) < 5$ and $\sigma(\mu_\delta) < 5 \text{ mas yr}^{-1}$ (37 stars were lost), and the accuracies of the Tycho-2 photometry are $\sigma(B_T) < 0.1^m$ and $\sigma(V_T) < 0.1^m$ (243 stars were lost). The final sample contains 27 440 stars.

More severe limitations, for example, $\sigma(\pi)/\pi < 0.2$ alongwith $\sigma(\mu_\alpha \cos \delta) < 3$ and $\sigma(\mu_\delta) < 3 \text{ mas yr}^{-1}$, leave 25 082 stars in the sample. In this case, all of the conclusions reached in this study remain valid and all of the categories of stars found are identified with no lesser confidence. However, a considerable number of bulge and halo stars that are few anyway are lost under severe limitations. Therefore, here we give preference to the mentioned mild limitations to exclude only the stars whose data do not allow them to be classified.

The dereddened color $(B_T - V_T)_0$ was calculated for each star:

$$(B_T - V_T)_0 = (B_T - V_T) - E(B_T - V_T), \quad (1)$$

where the reddening $E(B_T - V_T) = A_{V_T}/R_{V_T} \approx 1.1A_V/1.2R_V$. The coefficients in this formula were calculated by taking into account the extinction law from Draine (2003); the extinction A_V was calculated from our 3D analytical extinction model (Gontcharov 2009, 2012b) as a function of the trigonometric distance $r = 1/\pi$. and Galactic coordinates l and b , while the extinction coefficient R_V was calculated from the 3Dmap of its variations

as a function of the same coordinates (Gontcharov 2012a). The absolute magnitude M_{V_T} was calculated for each star from the formula

$$M_{V_T} = V_T + 5 - 5 \lg r - A_{V_T}. \quad (2)$$

The positions of our 27 440 sample stars on a Hertzsprung–Russell (H–R) diagram of the form “ $(B_T - V_T)_0 - M_{V_T}$ ” are shown in Fig. 1a. The sample under consideration contains almost all GCS stars with accurate data and a similar diagram for them is shown in Fig. 1b. It can be seen that, following the PCRV and in contrast to the GCS, all classes, including the main sequence (MS), the red giant clump and branch, supergiants, subgiants, subdwarfs, red dwarfs, and one white dwarf, are represented in the sample. The line indicates the theoretical zero-age main sequence (ZAMS) from the Padova database of evolutionary tracks and isochrones (<http://stev.oapd.inaf.it/cmd>; Bressan et al. 2012), which was fitted with an accuracy (about 0.1m) sufficient for the subsequent analysis by the polynomial

$$Y = 5.9X^5 - 19.34X^4 + 21.1X^3 - 8.8X^2 + 5.8X + 1.7, \quad (3)$$

where $X = (B_T - V_T)_0$, $Y = M_{V_T}$. The cross indicates typical errors, $\sigma((B_T - V_T)_0) = 0.02^m$ and $\sigma(M_{V_T}) = 0.5^m$, for an individual star. It can be seen that cloud of points of MS stars is located mainly to the right and above the ZAMS, as it must be. However, in the range $0^m < (B_T - V_T)_0 < 0.35^m$, which roughly corresponds to the spectral type AV, the well-known deviation of the cloud from the shown ZAMS is noticeable. This deviation will be discussed in a separate study.

The Galactic orbits of the stars under consideration were calculated using the Galactic potential from Fellhauer et al. (2006) and Helmi et al. (2006): $\Phi = \Phi_{halo} + \Phi_{disk} + \Phi_{bulge}$. In this case,

- the halo was represented by a potential dependent on the cylindrical Galactic coordinates R and Z as $\Phi_{halo}(R, Z) = \nu_0^2 \ln(1 + R^2/d^2 + Z^2/d^2)$, where $\nu_0 = 134 \text{ km s}^{-1}$ and $d = 12 \text{ kpc}$;

- the disk was represented by the potential from Miyamoto and Nagai (1975) as a function of the same coordinates: $\Phi_{disk}(R, Z) = -GM_d(R^2 + (b + (Z^2 + c)^{1/2})^2)^{-1/2}$, where the disk mass $M_d = 9.3 \cdot 10^{10} M_\odot$, $b = 6.5 \text{ kpc}$, and $c = 0.26 \text{ kpc}$;

- the bulge was represented by the potential from Hernquist (1990): $\Phi_{bulge}(R) = -GM_b/(R + a)$, where the bulge $M_b = 3.4 \cdot 10^{10} M_\odot$ and $a = 0.7 \text{ kpc}$.

The Galactic rotation velocity at $r = 8 \text{ kpc}$ for the Sun was taken to be 220 km s^{-1} . The solar motion relative to the local standard of rest was taken to be $(U = 10, V = 11, W = 7) \text{ km s}^{-1}$ based on the results by Bobylev and Bajkova (2010) in agreement with the results by Schönrich et al. (2010) and Gontcharov (2012d).

The key characteristics of the calculated orbits are the peri- and apogalactic distances designated below as r_{min} and r_{max} , respectively, the orbital eccentricity e , and the largest distance of the orbit from the Galactic plane Z_{max} .

3 ESTIMATING THE INFLUENCE OF ERRORS

Let us estimate the influence of errors in V_r and μ on r_{min} , r_{max} , e and Z_{max} .

For double and multiple stars, the observed component or photocenter can move over the celestial sphere nonlinearly. For visual binary stars (resolved systems), this occurs

due to the orbital motion of the components or because one of them falls or does not fall within the field of view. For astrometric binaries (unresolved systems), this occurs due to the orbital motion of the system's photocenter relative to the barycenter. In both cases, the variability of at least one of the components can also have an effect. Although Vityazev et al. (2003) showed an insignificant influence of the orbital motions in star pairs on the stellar kinematics, let us estimate this influence by a different method.

The proper motions from catalogues with a large difference of epochs (e.g., more than 50 years for Tycho-2), a small difference of epochs (e.g., 3.5 years for Hipparcos), and the orbital motions were compared, for example, by Gontcharov et al. (2001) and Gontcharov and Kiyaveva (2002). It follows from this comparison that precisely the orbital motions are responsible for the large differences of μ in such catalogues as Hipparcos and Tycho-2 and that here it is more appropriate to use μ from Tycho-2. Their replacement by μ from Hipparcos when calculating the Galactic orbits just reflects the influence of the orbital motions in star pairs. The standard deviation of the differences between μ from Tycho-2 and Hipparcos for the stars under consideration is 1.8 mas yr^{-1} . The values of r_{min} , r_{max} , e and Z_{max} calculated using μ from Tycho-2 and r'_{min} , r'_{max} , e' and Z'_{max} calculated using μ from Hipparcos differ insignificantly: the standard deviations of the differences are $\sigma(r'_{max} - r_{max}) = 0.15 \text{ kpc}$, $\sigma(r'_{min} - r_{min}) = 0.02$, $\sigma(e' - e) = 0.01$, $\sigma(Z_{max} - Z'_{max}) = 0.02 \text{ kpc}$. Thus, although the Galactic orbital parameters for an individual star can be strongly affected by inaccurate/incomplete knowledge of its duplicity, the latter does not affect the statistical results of analyzing the Galactic orbits for a sample of ten or more stars.

When creating the PCRV, we found and took into account numerous and various physically justified dependences of V_r on it itself (probably primarily due to the scale error and the tilt of the focal plane when the distances between spectral lines were measured), on the $(B - V)$ color (probably primarily due to the differences between the measured and comparison spectra), and on the celestial coordinates α and δ (probably primarily due to the seasonal correlations between the celestial coordinates, the instrument's temperature, and the hour angle) in the original catalogues. For the original catalogues produced with similar instruments, similar systematic dependences were found in the PCRV. For example, the GCS and the results by de Medeiros and Mayor (1999) obtained with the identical CORAVEL spectrometers give coincident (within the accuracy limits) dependences of V_r on V_r , $(B - V)$, and α , as shown in Fig. 1 and Table 3 from Gontcharov (2006).

To model the influence of systematic errors in V_r , we calculated the orbits using a radial velocity distorted by errors:

$$V'_r = V_r + 2.52(B - V)^2 - 4.7(B - V) + 0.002V_r - 0.034\alpha - 0.04 \cos(\alpha + 0.7) + 1.88, \quad (4)$$

where V'_r and V_r are in km s^{-1} , $(B - V)$ is in magnitudes, and α is in radians. This formula reflects the errors found by Gontcharov (2006) in the GCS (an error was made in the text of the paper when the PCRV was published but not in the calculations: there should be $\cos(\alpha + 0.7)$ or $\cos(\alpha + 40^\circ)$ if the phase is in degrees instead of the published $\cos(\alpha - 40^\circ)$).

For the stars under consideration, the difference $|V'_r - V_r|$ from Eq. (4) can reach 2.3 km s^{-1} , which is approximately triple the median random error of V_r in the PCRV.

In our analysis, it makes sense to model the errors by Eq. (4) instead of using r_{min} , r_{max} , e and Z_{max} directly from the GCS, because these errors, as follows from our comparison of the GCS and the results by de Medeiros and Mayor (1999), also extend to the spectral types of stars earlier than F and later than G, which are virtually absent in the

GCS. In addition, the GCS results differ from the results of this study due to the differences not only in radial velocities but also in distances and extinction estimates, while we want to estimate the influence of only the errors in V_r .

The values of r_{min} , r_{max} , e and Z_{max} calculated using V_r and r'_{min} , r'_{max} , e' and Z'_{max} calculated using V'_r differ insignificantly for disk stars and markedly for halo stars, i.e., for stars with $r_{max} > 20$ and $Z_{max} > 4$. Consequently, the systematic errors of V_r affect the statistical results of analyzing the Galactic orbits of only the halo stars due to the small number of these stars in the sample. Thus, either a careful allowance for the systematic errors in V_r or sample completeness is needed to analyze the Galactic orbits of halo stars. Obviously, both conditions are violated in most of the previous studies of the halo orbits.

The mean value of the differences $\overline{r'_{max} - r_{max}}$, just as of the remaining orbital parameters, is zero. The standard deviations of the differences are $\sigma(r'_{max} - r_{max}) = 0.44$ kpc, $\sigma(r'_{min} - r_{min}) = 0.03$ kpc, $\sigma(e' - e) = 0.01$, $\sigma(Z'_{max} - Z_{max}) = 0.08$ kpc. A direct comparison of the orbital parameters from the GCS with those obtained here gives the mean values of the differences $\Delta r_{max} = 0.19$ kpc, $\Delta r_{min} = 0.08$ kpc, $\Delta e = 0.005$, $\Delta Z_{max} = -0.05$ kpc and their standard deviations $\sigma(\Delta r_{max}) = 0.35$ kpc, $\sigma(\Delta r_{min}) = 0.19$ kpc, $\sigma(\Delta e) = 0.02$, $\sigma(\Delta Z_{max}) = 0.15$ kpc. The noticeable differences between the modeling and the real GCS for $\sigma(r'_{min} - r_{min}) = 0.03$ versus $\sigma(\Delta r_{min}) = 0.19$ kpc and $\sigma(Z'_{max} - Z_{max}) = 0.08$ versus $\sigma(\Delta Z_{max}) = 0.15$ kpc are caused by the differences in distance and extinction estimates in this study compared to the GCS.

Here, we considered the main sources of systematic errors and, in addition, can estimate the random errors of the orbital parameters based on the errors in the observed quantities. In our subsequent analysis of the results, typical total error estimates are marked in the figures. They are determined mainly not by the random errors of the velocities but by their systematic errors, which should not be ignored.

4 RESULTS

Figures 1c and 1d show the positions of the sample and GCS stars, respectively, on the “ $(B_T - V_T)_0 - e$ ” diagram; Figs. 1e and 1f, 1g and 1h, and 1i and 1j show their positions on the “ $(B_T - V_T)_0 - r_{max}$ ”, “ $(B_T - V_T)_0 - r_{min}$ ”, and “ $(B_T - V_T)_0 - Z_{max}$ ” diagrams, respectively (the orbital parameters in Figs. 1d, 1f, 1h, and 1j were taken directly from the GCS).

It can be seen that all categories of stars except FV–GV are represented in the GCS much more poorly than they are in the sample under consideration, although the distribution has the same structure.

The dashed lines in Figs. 1c, 1e, 1g, and 1i indicate an approximate separation of the stars into six categories by their evolutionary status and membership in Galactic subsystems. Below, we analyze separately

- 5377 stars with $(B_T - V_T)_0 < 0.3^m$, below referred to as the OA subsample),
- 12 600 stars with $0.3^m < (B_T - V_T)_0 < 0.85^m$ (mostly FV–GV, below referred to as the FG subsample),
- 9463 stars with $(B_T - V_T)_0 > 0.85^m$ (mostly K–M with a large fraction of giants, below referred to as the KM subsample).

The results for the FG subsample can be compared with those from the GCS. Each subsample was divided in the figure by the horizontal dashed line approximately into stars

with eccentric orbits (halo and bulge stars) and with more circular orbits (disk stars, so far without any separation into the thin and thick disks, given that this separation has recently been called into question (Bovy et al. 2012)).

The present-day theory of stellar evolution suggests that hot subdwarfs (evolved stars mainly with reactions in the helium core, i.e., on the horizontal giant branch), cool subdwarfs (unevolved low metallicity dwarfs near the MS) and low-mass branch giants dominate among the high-eccentricity stars of the OA, FG, and KM subsamples, respectively. It can be seen that there are much more high-eccentricity stars in the FG subsample than in the remaining subsamples. This could not be affected by the sample selection in r and V_T , because the absolute magnitudes of hot and cool subdwarfs are approximately equal, while giants are seen even at a greater distance. Most of the high-eccentricity stars we observe theoretically have a mass smaller than 0.8 Solar mass. Therefore, the predominance of cool subdwarfs is explained by the fact that only the oldest and low-mass metal-poor stars have managed to become giants in the lifetime of the Galaxy, while the majority remain near the MS.

For nonsingle stars in Hipparcos, the orbital parameters, π and μ were determined jointly from directly observed quantities, the abscissas on the reference great circle. The orbital motion can distort the observed π predominantly in the direction of its increase. When the angular measure is converted to the linear one, the measured μ then turn out to be smaller than the true ones due to the erroneous distance. As a result, the calculated e is larger than the true one and disk stars demonstrate the orbits of halo or bulge stars. This effect should manifest itself irrespective of $(B_T - V_T)_0$. However, the significantly nonuniform distribution of halo and bulge stars on $(B_T - V_T)_0$ seen in Fig. 1 suggests that this effect is absent.

The following effects are less pronounced in Fig. 1 but important. The small number of high-eccentricity stars in the range $0.1^m < (B_T - V_T)_0 < 0.25^m$ corresponds to the theory of subdwarfs (Gontcharov et al. 2011). A local minimum in the scatter of orbital parameters for disk stars is reached at $(B_T - V_T)_0 \approx 0.1^m$, while this scatter in the range $0.3^m < (B_T - V_T)_0 < 0.4^m$ increases sharply.

Applying the more stringent star selection criteria $\sigma(\pi)/\pi < 0.2$, $\sigma(\mu_\alpha \cos \delta) < 3$ and $\sigma(\mu_\delta) < 3 \text{ mas yr}^{-1}$, which leave only 25 082 stars in the sample, does not change qualitatively the distribution of stars on the diagrams of Figs. 1a, 1c, 1e, 1g, and 1i. As an example, Fig. 2 presents the “ $(B_T - V_T)_0 - r_{min}$ ” (a) and “ $(B_T - V_T)_0 - Z_{max}$ ” (b) diagrams for 25 082 sample stars with the above stringent selection criteria, which are worth comparing with Figs. 1g and 1i, respectively.

Comparison of Orbital Parameters

Figure 3 shows the distribution of stars from the OA subsample on the (a) “ $r_{max} - e$ ”, (b) “ $Z_{max} - e$ ”, (c) “ $r_{min} - e$ ”, (d) “ $r_{min} - Z_{max}$ ”, (e) “ $r_{max} - r_{min}$ ”, and (f) “ $r_{max} - Z_{max}$ ” diagrams. Here, the limitations due to the sample selection by r and V_T are noticeable. For example, the selection in Fig. 3c manifests itself in the correlation between r_{min} and e . Despite the selection, some conclusions are possible.

As expected, the overwhelming majority of stars from the OA subsample are young low-eccentricity stars. Indeed, Gontcharov (2012d) found a correlation between the age and $(B_T - V_T)_0$ for stars near the MS with $(B_T - V_T)_0 < 0.7^m$:

$$T = 0.42e^{3.86(B_T - V_T)_0}, \quad (5)$$

which agrees well with that from the GCS data. According to this formula, the OA-subsample stars near the MS ($> 80\%$ of the subsample) have ages younger than 1.34 Gyr and nearly circular orbits ($e < 0.1$, $r_{max} < 10$ kpc, $r_{min} > 6$ kpc, $Z_{max} < 0.3$ kpc) and, thus, belong to the thin disk. A nonuniformity of the distribution of these stars is noticeable in Fig. 3e. It is caused primarily by selection in favor of nearby stars and, accordingly, by a predominance of stars with $r_{min} \approx 8$ and $r_{max} \approx 8$ kpc. The additional star density variations in the densely populated region of Fig. 3e are caused by the influence of the dynamical streams of disk stars or super clusters considered, for example, in the GCS, by Famaey et al. (2005) and Gontcharov (2012c, 2012d). The orbits of disk stars will be analyzed in detail separately.

The stars with $r_{min} < 2$ kpc and $e > 0.6$ are isolated in Fig. 3c in these parameters from the remaining ones and probably belong to the bulge. They are clearly divided into two groups: $7.8 < r_{max} < 9.5$ kpc and $10.5 < r_{max} < 12.2$ kpc. Selection could not eliminate the stars with intermediate r_{max} . Consequently, there is a physical cause of their absence. The separation of bulge stars into at least two groups should be admitted. However, there are different Z_{max} and Fe/H in each of these groups and the stars from the groups occupy approximately the same region of the H–R diagram, being known or suspected hot subdwarfs (the blue part of the horizontal branch). The only detected differences are related to the difference in r_{max} : the group with larger r_{max} has larger absolute values of the velocity component $|U| > 150$ km s $^{-1}$ and is in the longitude octants of the Galactic center and anticenter, while the group with smaller r_{max} has $|U| < 150$ km s $^{-1}$ and is at longitudes far from the center–anticenter line. The distribution of bulge stars in apogalactic distances are possibly subjected to density waves and other dynamical processes, as are the dynamical, predominantly radial Sirius (Ursa Major), Pleiades, Hyades, Coma Berenices, α Cet/Wolf 630, Hercules, and other streams (Gontcharov 2012c, 2012d). We then see two groups of bulge stars that are dynamically associated with two spiral arms. Judging by the mean r_{max} for the stars from these groups that are not too far from the Galactic plane, these arms are at Galactocentric distances of 8.3 (the arm near the Sun) and 11.6 kpc, respectively. Obviously, the group of stars with $3.3 < r_{min} < 4.5$ kpc and $0.3 < e < 0.42$ is then also isolated in Fig. 3c not by selection but by the dynamical processes that associated it with the arm nearest to us ($\overline{r_{max}} = 8.3$ kpc) and possibly the arm or a different structure near the perigalacticons of these stars.

Let us analyze the entire FG subsample and only the GCS stars from this subsample, respectively, in Figs. 4 and 5, which are similar to Fig. 3. The orbital parameters of the stars from the GCS rather than those that we calculated are used in Fig. 5.

Just as in the OA subsample, most of the stars in the FG subsample have $e < 0.3$, $6 < r_{min} < 8$ kpc, $8 < r_{max} < 10$ kpc, and $Z_{max} < 0.5$ kpc, i.e., these are disk stars with moderately eccentric orbits. Formula (5), which gives ages from 1.34 to 11 Gyr for these stars, is valid for them.

As can be seen from our comparison of Figs. 4 and 5, the remaining stars, i.e., those with comparatively eccentric orbits, are represented in this study much better than in the GCS. A nonuniform distribution of stars with $e > 0.4$, $Z_{max} > 3$ kpc, and $r_{max} > 15$ kpc on the graphs of Fig. 4 is particularly noticeable. Because of the selection effect, not so much the regions of enhanced star density in the figure as the voids between them that are surrounded by stars and, therefore, that did not result from selection are important.

Judging by the almost complete absence of stars with $2 < Z_{max} < 3$ kpc, the boundary between the disk and halo as, respectively, the subsystem consisting mostly of stars born

in the Galaxy itself and the subsystem with a significant fraction of stars accreted from the Galaxy's disrupted satellites is clearly seen here. In support of this, we see a comparatively uniform distribution of disk stars ($2 < Z_{max} < 3$ kpc) and a nonuniform distribution of halo stars on the graphs. Two groups are identified with confidence among the latter:

the bulge–halo group with $e > 0.8$, $r_{min} < 1.5$ kpc, $3 < Z_{max} < 13$ kpc,

the halo group with $0.25 < e < 0.75$, $7 < r_{min} < 8$ kpc, $13 < r_{max} < 60$ kpc, $10 < Z_{max} < 21$ kpc,

and two more groups are identified with lesser confidence:

group 3 with $0.65 < e < 0.8$, $3.8 < Z_{max} < 5$ kpc, $1.5 < r_{min} < 3.6$ kpc,

group 4 with $0.4 < e < 0.55$, $3 < Z_{max} < 4.2$ kpc, $2.5 < r_{min} < 4.3$ kpc.

The uncertainty in identifying the groups stems from the fact that selection allows one to delineate not the boundaries of the groups but rather the boundaries of the voids between them. The bulge–halo group includes stars with their perigalacticons in the bulge and apogalacticons in the halo; the halo group includes typical halo stars with moderately eccentric orbits (at higher e , the perigalacticon falls into the bulge). Selection probably hid the halo stars with approximately circular orbits whose existence is not ruled out. Judging by the absence of intermediate stars with $1.5 < r_{min} < 7$ kpc, these groups are fairly isolated. Consequently, the stars with their apogalacticons in the halo can be divided into at least two groups. The difference in origin may be responsible for this division: the bulge–halo group was born in the Galaxy, while the halo group was accreted from disrupted satellites. The halo group is discussed below.

In the subsample under consideration, the bulge stars ($r_{min} < 2$ kpc) are much more numerous than in the GCS and are isolated from the remaining ones by voids on the graphs (though selection probably hid the bulge stars with less eccentric orbits). In addition to the mentioned bulge–halo group, a bulge–disk group with $Z_{max} < 2.2$ kpc, $r_{min} < 2$ kpc, and $e > 0.6$, i.e., with the apogalacticons in the disk, is identified among the stars with their perigalacticons in the bulge. Thus, we see the separation of the bulge stars into stars with disk and halo kinematics. Of particular importance is the absence of stars with intermediate $2 < Z_{max} < 3$ kpc between these groups, which cannot be the result of selection, i.e., the Galactic bulge combines the properties of the classical and disk-shaped bulges observed in other galaxies. It has an inhomogeneous structure and is probably a mixture of stars of different subsystems, as is hypothesized by Bensby et al. (2013) and in the papers cited by them.

Let us analyze the KM subsample in Fig. 6, which is similar to Figs. 3 and 4. Just as for the previous subsamples, most of the stars here ($r_{min} \approx 8$ kpc and $r_{max} \approx 8$ kpc) are disk stars with nearly circular orbits ($e < 0.3$, $Z_{max} < 2$ kpc), many of which belong to the dynamical streams or superclusters considered by Famaey et al. (2005). These streams manifest themselves particularly clearly in the nonuniform distribution of stars in the most densely populated part of Figs. 6a and 6e.

Just as for the FG subsample, a clear separation of the disk and halo at $Z_{max} \approx 3$ kpc and the separation of bulge stars ($r_{min} < 2$ kpc) into stars with disk ($Z_{max} < 1.5$ kpc) and halo ($Z_{max} > 4$ kpc) kinematics when only one star ($Z_{max} = 2.7$ kpc) is present in the interval can be seen for the KM subsample.

Orbital Parameters and Luminosity

Some categories of stars can be revealed by the deviation of their M_{V_T} from the ZAMS specified by Eq. (3). We will consider this deviation from the ZAMS .MVT to be negative for high-luminosity stars (e.g., branch giants) and positive for low luminosity stars (subdwarfs and white dwarfs).

Figure 7 shows the distribution of stars from the OA and KM subsamples on the following diagrams: “ $\Delta M_{V_T} - e$ ” (a) and (b), respectively; “ $\Delta M_{V_T} - r_{max}$ ” (c) and (d), respectively; “ $\Delta M_{V_T} - r_{min}$ ” (e) and (f), respectively; “ $\Delta M_{V_T} - Z_{max}$ ” (g) and (h), respectively. The solid vertical straight line marks .MVT = 0m and the dashed straight line marks .MVT = 1m, which corresponds to a 2. error in calculating M_{V_T} .

The star HIP 14754 with .MVT = 8.1m is the only white dwarf in the sample and is marked in the figure by the large circle.

The hot subdwarfs known from spectroscopy are marked in Figs. 3a, 3c, 3e, and 3g by the squares. Those of them that belong to the bulge ($r_{min} < 2$ kpc, $e > 0.6$) and two stars in the adjacent regions on the graphs ($2 < r_{min} < 3.5$ kpc, $0.4 < e < 0.6$) have a high luminosity ($\Delta M_{V_T} < 0^m$). As has been pointed out above, although their perigalacticons are in the bulge, judging by their kinematics they belong to the disk ($Z_{max} < 2.5$ kpc) or halo ($Z_{max} > 5$ kpc). On the contrary, the remaining known hot subdwarfs have a low luminosity ($\Delta M_{V_T} > 1^m$) and belong to the disk ($e < 0.4$, $Z_{max} < 1.5$ kpc). Following Gontcharov et al. (2011), this study confirms the existence of hot subdwarfs belonging to the Galactic thin disk in the solar neighborhood.

The hot subdwarfs are mostly stars of the horizontal branch. Its location on the H–R diagram depends on stellar metallicity, age, and mass. At solar metallicity, an age younger than 10×10^9 yr, and a mass of more than $0.8M_{\odot}$, the horizontal branch appears as a clump of giants at $0.9^m < (B_T - V_T)_0 < 1.5^m$. The horizontal branch becomes bluer with decreasing metallicity, increasing age, and decreasing mass to the extent that it turns out to be near the MS (blue horizontal branch) or even considerably bluer and lower than the MS (extremely blue horizontal branch) at $Fe/H < -0.8$, an age older than 13×10^9 yr, and a mass of less than $0.7M_{\odot}$. The corresponding stars are classified as sdA, sdB, and sdO. Thus, the main path of a star’s transformation into a hot subdwarf is a very low metallicity or an age older than that of the Galactic disk or very fast evolution due to the large mass loss on the giant branch. The less common paths of fast evolution of low-mass stars into the region of hot subdwarfs are related to mass transfer in a close star pair or other ways of the addition or removal of stellar material (for references, see Gontcharov et al. 2011). In any case, the existence of hot subdwarfs in the Galactic thin disk is far from an unambiguous explanation.

The group of thin-disk BV stars exhibiting a low luminosity that stands out in the figure with $\Delta M_{V_T} > 1^m$, $e \approx 0.05$, $r_{max} \approx 8.9$ kpc, $r_{min} \approx 7.8$ kpc, $Z_{max} \approx 0.05$ kpc may have a bearing on this problem. A detailed analysis of their characteristics from the Strasbourg database shows that they are all located in two regions of ongoing star formation, in Orion and near the star ρ Oph at distances $200 < r < 300$ pc. Both regions are known to exhibit small-scale variations in extinction coefficient R_V and interstellar extinction. For example, the popular 3D analytical extinction model by Arenou et al. (1992) for a field in Orion at this distance gives $A_V \approx 1^m$, while the 3D model by Gontcharov (2009, 2012b) gives $A_V \approx 0.5^m$. Both values are appreciably higher than the typical A_V estimates at these distances in other directions. It is the large value of

the adopted A_V that gives a very blue dereddened color $((B_T - V_T)_0$ for the stars under consideration according to Eq. (1). As a result, the stars turned out to be well below the MS in its blue part. It should be noted that the extinction model and the 3D map of R_V variations used give $E(B_T - V_T)$ for these stars that are smaller than other sources of estimates. Consequently, the derived low luminosity of these stars cannot be explained by the erroneous extinction and R_V estimates and should be investigated additionally. The most plausible explanations are: either the peculiarity of the medium and BV stars on the MS in the star-forming regions causes them to appear as low-luminosity stars on the H–R diagram, for example, due to an anomalously high extinction (this explanation appears more plausible) or they are actually not BV stars but hot sdB subdwarfs and the medium of the star-forming regions aids the formation of such stars. Indeed, an especially intense mass loss on the giant branch, including that due to an external stellar wind at small distances between the stars, the presence of a close component for mass transfer, and a high spatial and physical density of clouds supplying hydrogen into the stellar envelope that has already used it up contribute to the formation of a hot subdwarf.

The subdwarfs from the OA subsample will be studied in detail separately after the collection of data on their metallicity.

In the KM subsample in Figs. 7b, 7d, 7f, and 7h, we see the separation into giants ($\Delta M_{V_T} < -2^m$) and dwarfs ($\Delta M_{V_T} > -2^m$). The overwhelming majority of both giants and dwarfs belong to the disk ($e < 0.6$, $r_{min} > 2$ kpc, $Z_{max} < 2.5$ kpc). Almost all of the remaining ones belong to the bulge ($r_{min} < 2$ kpc). Only two dwarfs have $\Delta M_{V_T} > 1^m$ and, thus, are probably cool low-metallicity subdwarfs in the disk. As expected, the KM subsample contains almost no cool subdwarfs due to selection. However, the tendency for ΔM_{V_T} to increase with increasing e and decreasing r_{min} caused by a drop in mean metallicity should be noted for both bulge giants and dwarfs ($e > 0.6$, $r_{min} < 2$ kpc). It can be seen that this tendency is opposite to that for the OA subsample and reflects a different nature of the low-luminosity stars: these are dwarfs and branch giants in the KM subsample and giants of the blue part of the horizontal branch in the OA subsample.

In Fig. 8, which is similar to Fig. 7, we will analyze the entire FG subsample (see Figs. 8a, 8c, 8e, 8g) and the GCS stars from this subsample (see Figs. 8b, 8d, 8f, 8h). It can be seen that with regard to the disk stars ($e < 0.3$, $r_{min} > 3$ kpc, $Z_{max} < 2$ kpc), the distribution of the subsample stars in the figure virtually coincides with that of the GCS stars. However, with regard to the remaining stars, the subsample is more complete than the GCS. Dwarfs ($\Delta M_{V_T} > -2^m$) and giants ($\Delta M_{V_T} < -2^m$) with their perigalacticons in the bulge ($r_{min} < 2$ kpc) and apogalacticons in the halo ($Z_{max} > 2$ kpc) dominate among the stars outside the disk. In contrast to the disk stars with $\overline{\Delta M_{V_T}} < 0^m$, they have a low luminosity ($\overline{\Delta M_{V_T}} > 0^m$). This makes them similar to the KM subsample stars and distinguishes them from the hot subdwarfs of the OA subsample.

There are five halo stars with their perigalacticons outside the bulge in the FG subsample: the previously mentioned halo group. Their small number in the subsample is explained by the fact that the FG dwarfs have a low luminosity and are not visible from afar, while the horizontal-branch giants with $((B_T - V_T)_0 < 0.85^m$, i.e., with $Fe/H < -0.6$, are very few. However, halo giants are absent altogether in the KM subsample, because only giants with $Fe/H > -0.6$ may turn out to be in the interval $(B_T - V_T)_0 > 0.85^m$, and there are probably no such stars in the halo. Out of these five stars, HIP 103311 is a dwarf, while HIP 92 167, 85 855, 71 458, and 62 747 are horizontal-branch low-metallicity giants. All of their characteristics confirm that they belong to the halo, with the interval

$-5.2^m < \Delta M_{V_T} < -2.9^m$ populated by these stars just corresponding to the location of the horizontal branch relative to the MS for the F and G types. Therefore, the entire isolated group of stars with $-5.2^m < \Delta M_{V_T} < -2.4^m$, $Z_{max} > 2$ kpc, and $r_{max} > 12$ kpc probably consists of horizontal-branch low-metallicity giants. It can be seen from Fig. 8 that these stars are absent in the GCS and were first detected as an isolated group in this study.

Gontcharov et al. (2011) found no cool disk subdwarf (with $e < 0.4$). The GCS also gives few stars with $e < 0.4$ and $\Delta M_{V_T} > 1$. The FG subsample contains several such stars. Analysis of their characteristics from the Strasbourg database shows that they are all young nonsingle and variable stars in starforming regions rather than subdwarfs.

5 CONCLUSIONS

We analyzed the Galactic orbits of 27 440 stars of all classes with accurate α , δ and $\pi > 3$ mas from the Hipparcos catalogue, μ from the Tycho-2 catalogue, and V_r from the Pulkovo Compilation of Radial Velocities (PCRV). The detection of systematic errors in V_r when the PCRV was created and the noticeable difference between μ from Tycho-2 and Hipparcos caused by the orbital motions in star pairs forced us to estimate the influence of these errors on orbital parameters: the peri- and apogalactic distances r_{min} and r_{max} , the eccentricity e , and the largest distance of the orbit from the Galactic plane Z_{max} . We found that the errors of μ due to the duplicity of stars are tangible only in the statistics of orbital parameters for very small samples (fewer than 10 stars), while the errors of the radial velocities are noticeable in the statistics of orbital parameters for stars far from the Sun, i.e., halo stars. The sample considered here is much more representative than the Geneva–Copenhagen survey with regard to F–G stars that do not belong to the disk and exceeds considerably any other sample for O–A and K–M stars. This allows our study to be considered as the largest survey of Galactic orbits in the solar neighborhood to date. Note that the derived orbital parameters agree with those from the GCS for the same stars.

Here, we analyzed the distribution of stars in the multidimensional space of orbital parameters, dereddened colors, and absolute magnitudes so far almost without invoking the stellar metallicities and ages (this will be done in a subsequent paper). Since the sample is limited in parallax and apparent magnitude, many of the groups of stars (for example, halo stars with circular orbits) cannot appear in it. However, even our analysis of selection-free regions of this multidimensional space allowed us to establish a nonuniformity of the distribution of stars in it and to identify several groups. First of all, this study allowed the radius of the bulge to be determined (2 kpc) and showed that the bulge and the halo are not homogeneous subsystems of the Galaxy. The stars with their perigalacticons in the bulge are clearly divided into stars with their apogalacticons in the halo and the disk, while the stars with their apogalacticons in the halo are divided into stars with their perigalacticons in the bulge and the disk. Thus, instead of the evidence for the membership of a star in a subsystem, the evidence for which subsystem the perigalacticon and apogalacticon of its orbit are located in is more informative. Therein may lie the difference in the origin of stars: in the Galaxy or in the accreted satellites.

The nonuniformity of the distribution of bulge stars with their apogalacticons in the disk in apogalactic distances may be explained by the dynamical association of these stars

with spiral arms.

Our investigation showed that using Galactic orbits is promising. In future, they can be applied to calculate the statistical characteristics of the disk and, by invoking the stellar metallicities and ages, for a detailed analysis of the bulge and the halo.

6 ACKNOWLEDGMENTS

We used resources from the Strasbourg Astronomical Data Center (Centre de Données astronomiques de Strasbourg). This study was supported by Program P21 of the Presidium of the Russian Academy of Sciences and the Ministry of Education and Science of the Russian Federation under contract no. 8417.

7 REFERENCES

1. F. Arenou, M. Grenon, and A. Gomez, *Astron. Astrophys.* 258, 104 (1992).
2. T. Bensby, J. C. Yee, S. Feltzing, et al., *Astron. Astrophys.*
3. V. Bobylev and A. Bajkova, *Mon. Not. R. Astron. Soc.* 408, 1788 (2010).
4. J. Bovy, H.-W. Rix, and D. W. Hogg, *Astrophys. J.* 751, 131 (2012).
5. A. Bressan, P. Marigo, L. Girardi, et al., *Mon. Not. R. Astron. Soc.* 427, 127 (2012).
6. B. T. Draine, *Ann. Rev. Astron. Astrophys.* 41, 241 (2003).
7. B. Famaey, A. Jorissen, X. Luri, et al., *Astron. Astrophys.* 430, 165 (2005).
8. M. Fellhauer, V. Belokurov, N. W. Evans, et al., *Astrophys. J.* 651, 167 (2006).
9. G. A. Gontcharov and O. V. Kiyayeva, *Astron. Lett.* 28, 261 (2002).
10. G. A. Gontcharov, *Astron. Lett.* 32, 759 (2006).
11. G. A. Gontcharov, *Astron. Lett.* 35, 780 (2009).
12. G. A. Gontcharov, *Astron. Lett.* 38, 12 (2012a).
13. G. A. Gontcharov, *Astron. Lett.* 38, 87 (2012b).
14. G. A. Gontcharov, *Astron. Lett.* 38, 694 (2012c).
15. G. A. Gontcharov, *Astron. Lett.* 38, 771 (2012d).
16. G. A. Gontcharov, A. A. Andronova, O. A. Titov, et al., *Astron. Astrophys.* 365, 222 (2001).
17. G. A. Gontcharov, A. T. Bajkova, P. N. Fedorov, et al., *Mon. Not. R. Astron. Soc.* 413, 1581 (2011).
18. A. Helmi, J. F. Navarro, B. Nordström, et al., *Mon. Not. R. Astron. Soc.* 365, 1309 (2006).
19. L. Hernquist, *Astrophys. J.* 356, 359 (1990).
20. E. Hog, C. Fabricius, V. V. Makarov, et al., *Astron. Astrophys.* 355, L27 (2000).
21. J. Holmberg, B. Nordström, and J. Andersen, *Astron. Astrophys.* 475, 519 (2007).
22. J. Holmberg, B. Nordström, and J. Andersen, *Astron. Astrophys.* 501, 941 (2009).
23. F. van Leeuwen, *Astron. Astrophys.* 474, 653 (2007).
24. J. R. de Medeiros and M. Mayor, *Astron. Astrophys. Suppl. Ser.* 139, 433 (1999).
25. M. Miyamoto and R. Nagai, *Publ. Astron. Soc. Jpn.* 27, 533 (1975).

26. B. Nordström, M. Mayor, J. Andersen, et al., *Astron. Astrophys.* 418, 989 (2004).
27. M. Perryman, *Astronomical Applications of Astrometry* (Cambridge Univ. Press, Cambridge, 2009).
28. R. Schönrich, J. Binney, and W. Dehnen, *Mon. Not. R. Astron. Soc.* 403, 1829 (2010).
29. V. V. Vityazev, V. V. Bobylev, and G. A. Gontcharov, *Vestn. SPb. Univ., Ser. 1, No. 4* (25), 111 (2003). 549, 147 (2013).

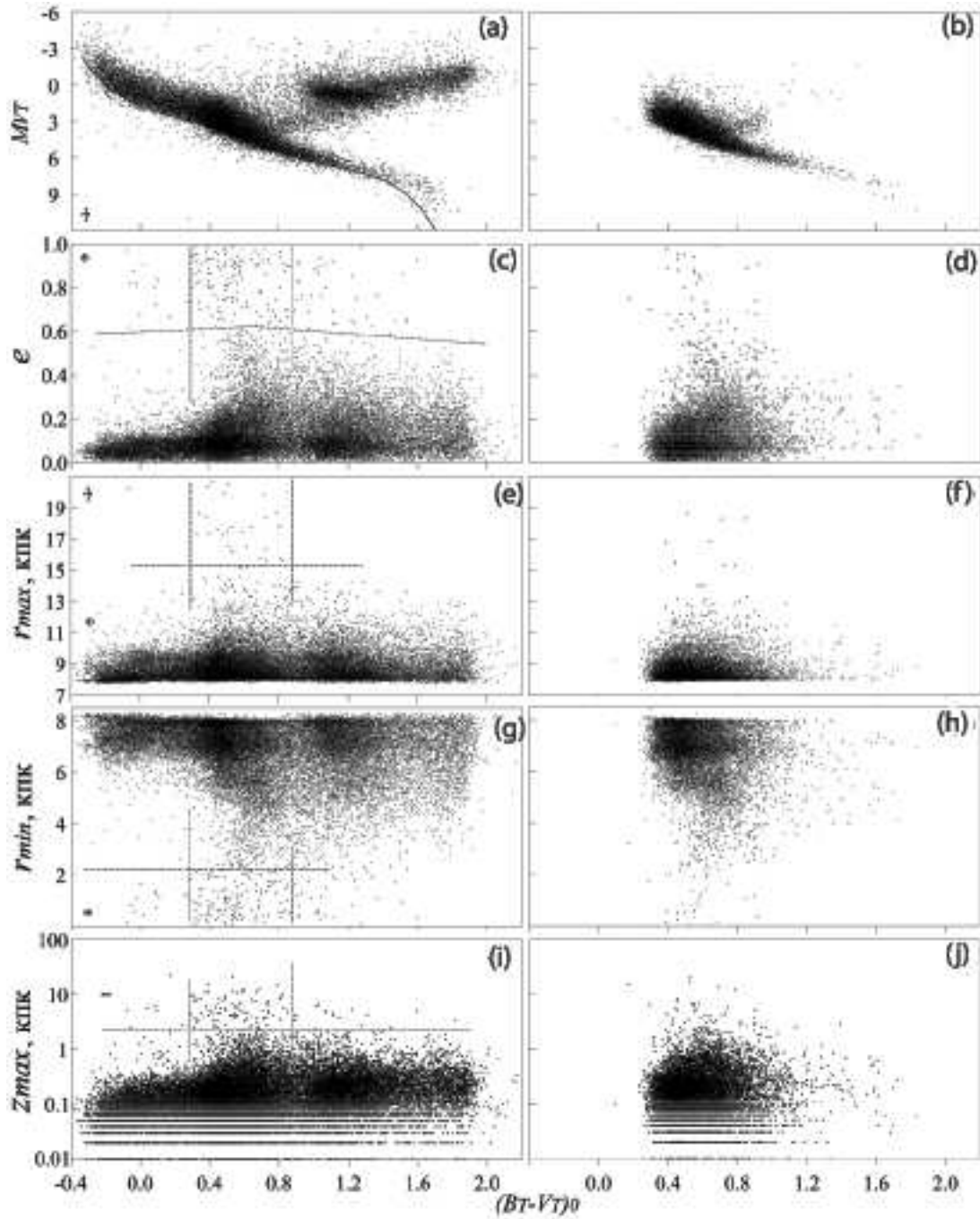


Figure 1: “ $(B_T - V_T)_0 - M_{V_T}$ ” diagram for the sample (a) and GCS (b) stars (the line indicates the theoretical ZAMS); “ $(B_T - V_T)_0 - e$ ” for the sample (c) and GCS (d) stars; “ $(B_T - V_T)_0 - r_{max}$ ” for the sample (e) and GCS (f) stars; “ $(B_T - V_T)_0 - r_{min}$ ” for the sample (g) and GCS (h) stars; “ $(B_T - V_T)_0 - Z_{max}$ ” for the sample (i) and GCS (j) stars. The crosses near the vertical axes indicate typical errors in the data for a star. The dashed lines are discussed in the text.

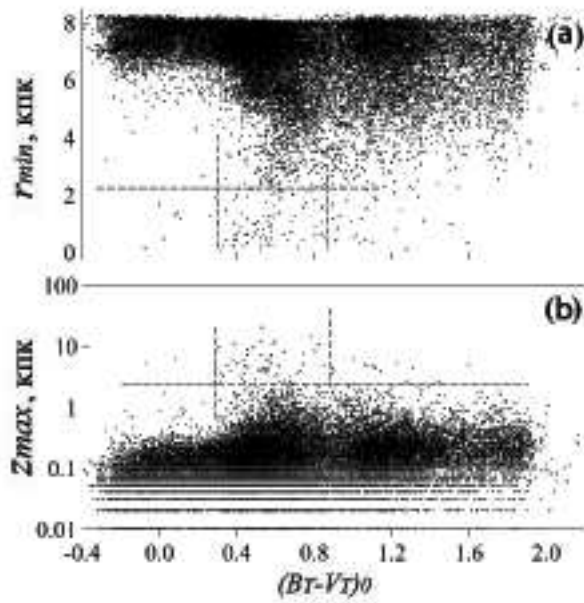


Figure 2: “ $(B_T - V_T)_0 - r_{min}$ ” (a) and “ $(B_T - V_T)_0 - Z_{max}$ ” (b) diagrams for 25 082 sample stars with $\sigma(\pi)/\pi < 0.2$, $\sigma(\mu_\alpha \cos \delta) < 3$, and $\sigma(\mu_\delta) < 3 \text{ mas yr}^{-1}$. The dashed lines were taken from Fig. 1.

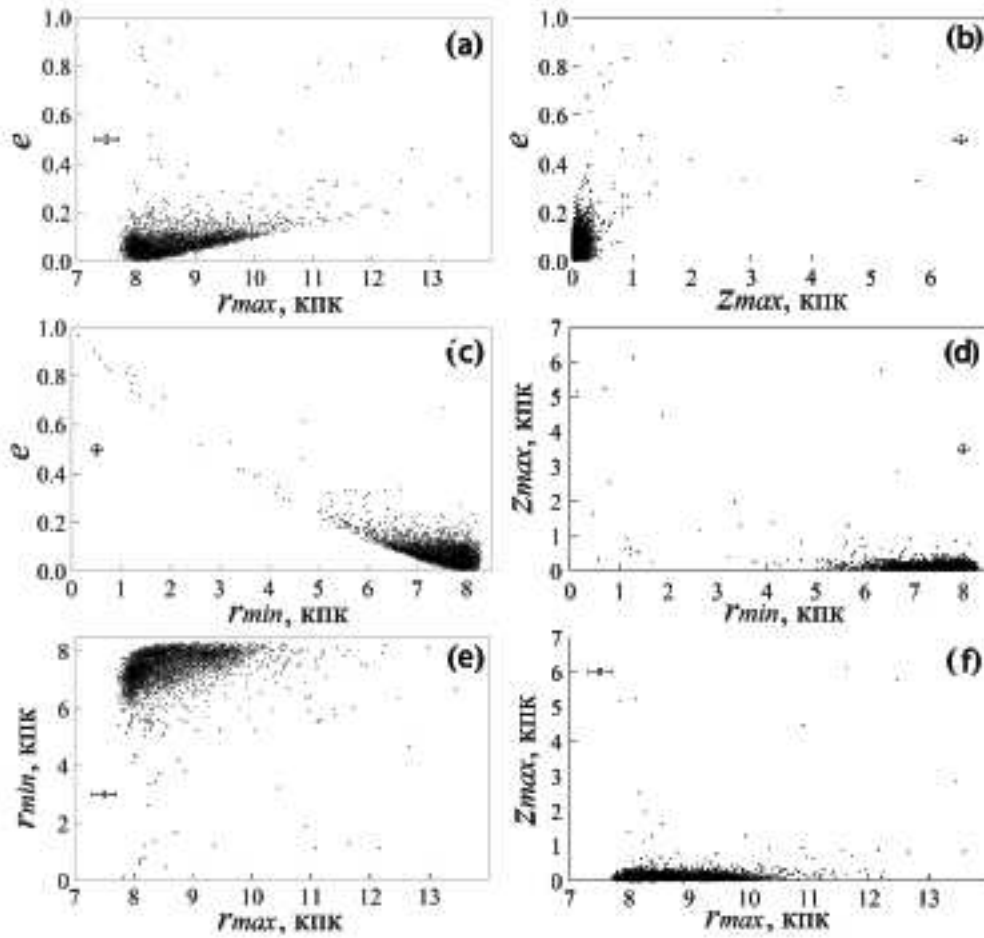


Figure 3: Positions of 5377 stars from the OA subsample on the (a) “ $r_{max} - e$ ”, (b) “ $Z_{max} - e$ ”, (c) “ $r_{min} - e$ ”, (d) “ $r_{min} - Z_{max}$ ”, (e) “ $r_{max} - r_{min}$ ”, and (f) “ $r_{max} - Z_{max}$ ” diagrams. The crosses indicate typical errors for a star.

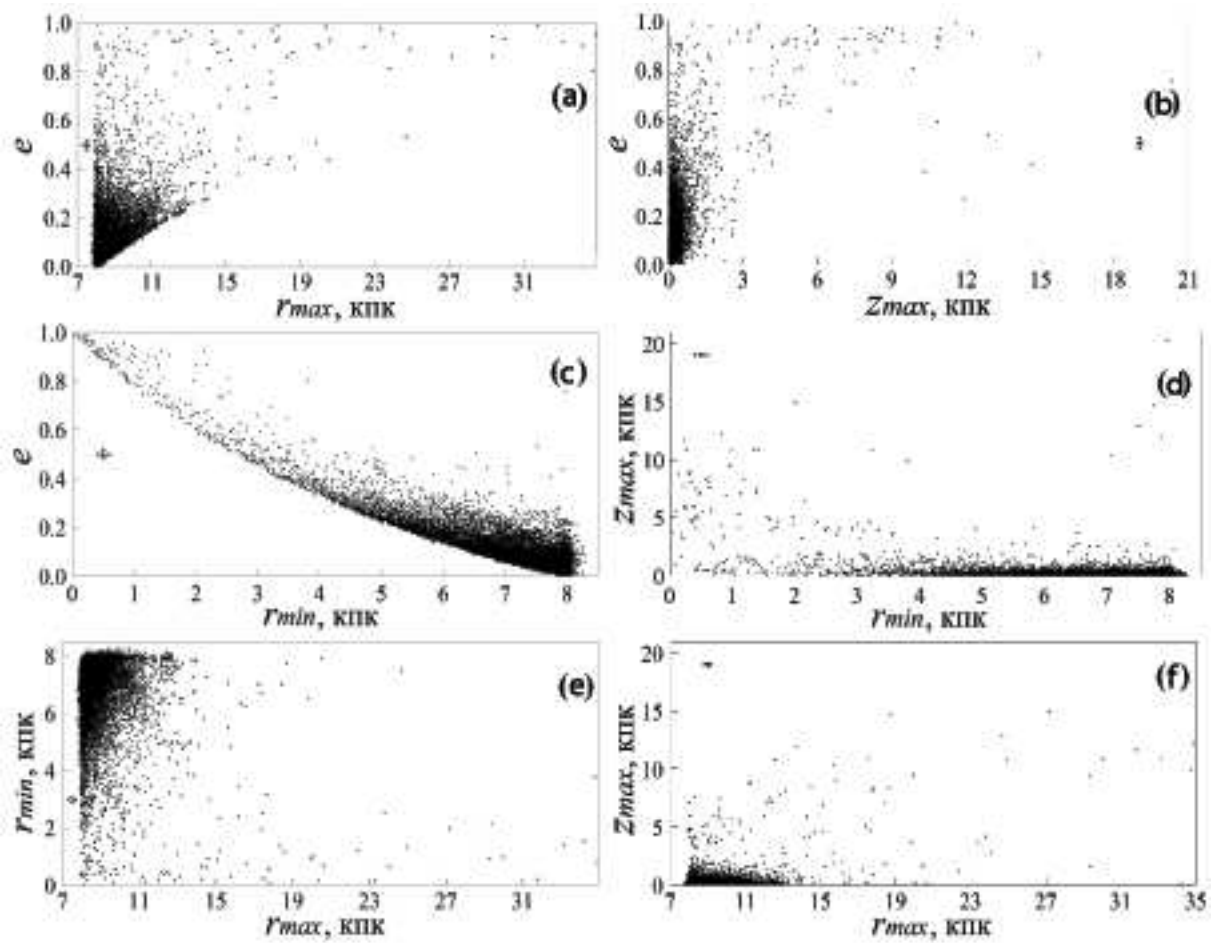


Figure 4: Same as Fig. 3 for 12 600 stars from the FG subsample.

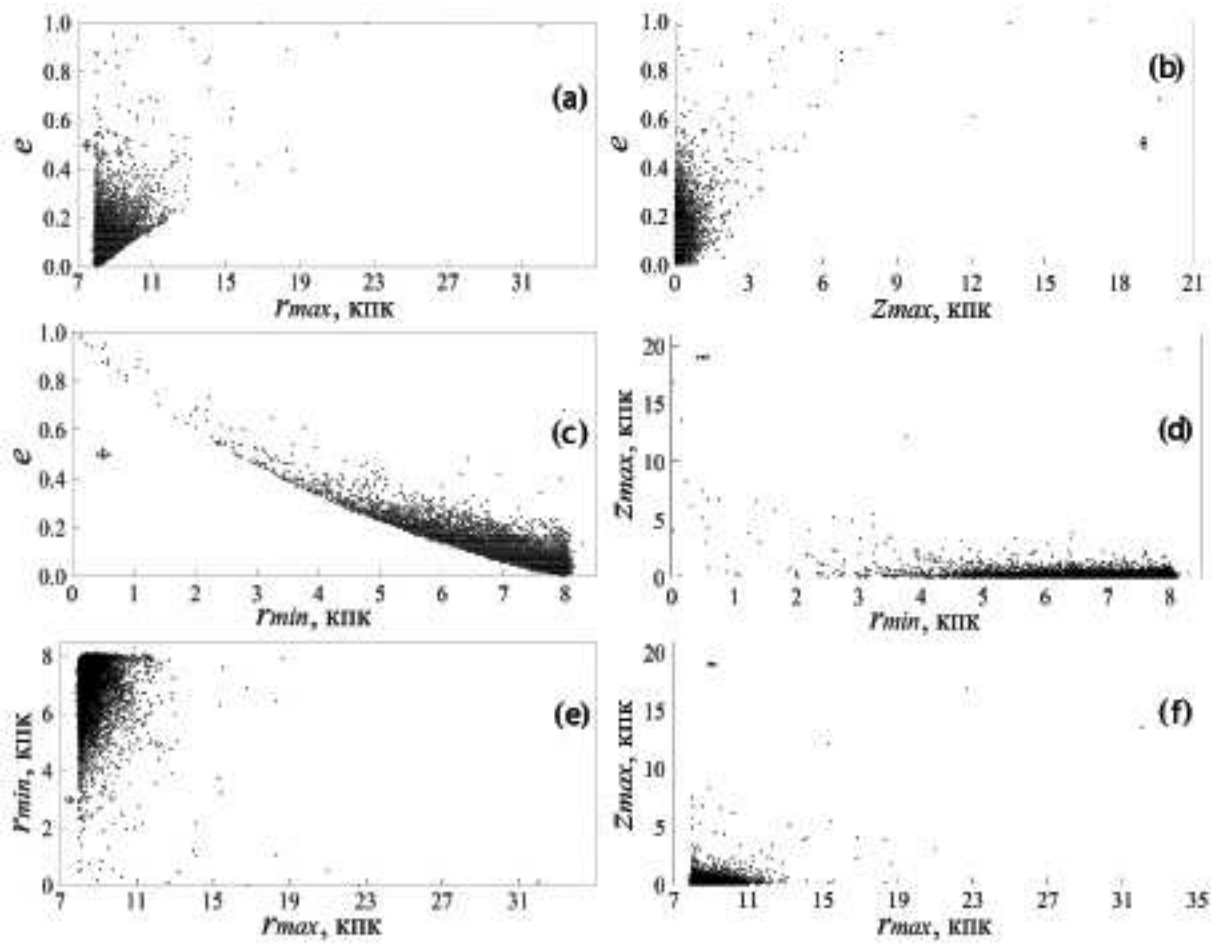


Figure 5: Same as Fig. 3 for the GCS stars from the FG subsample.

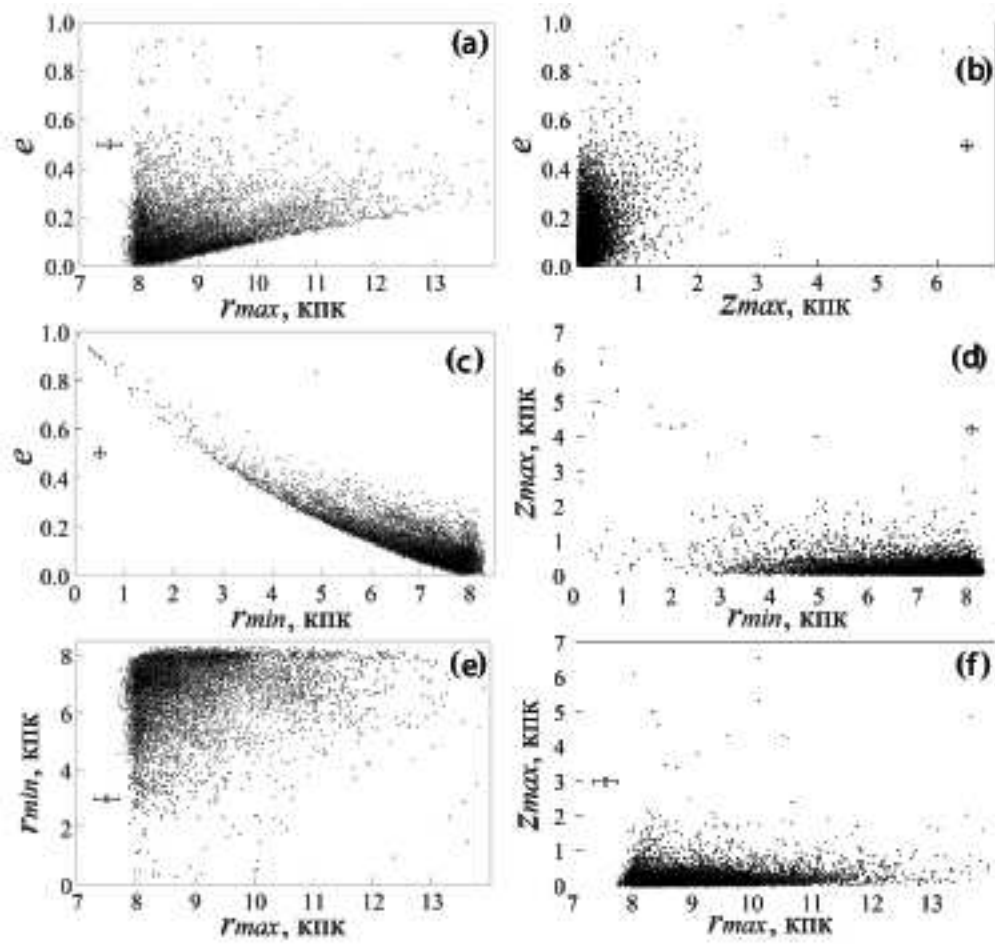


Figure 6: Same as Fig. 3 for 9463 stars from the KM subsample.

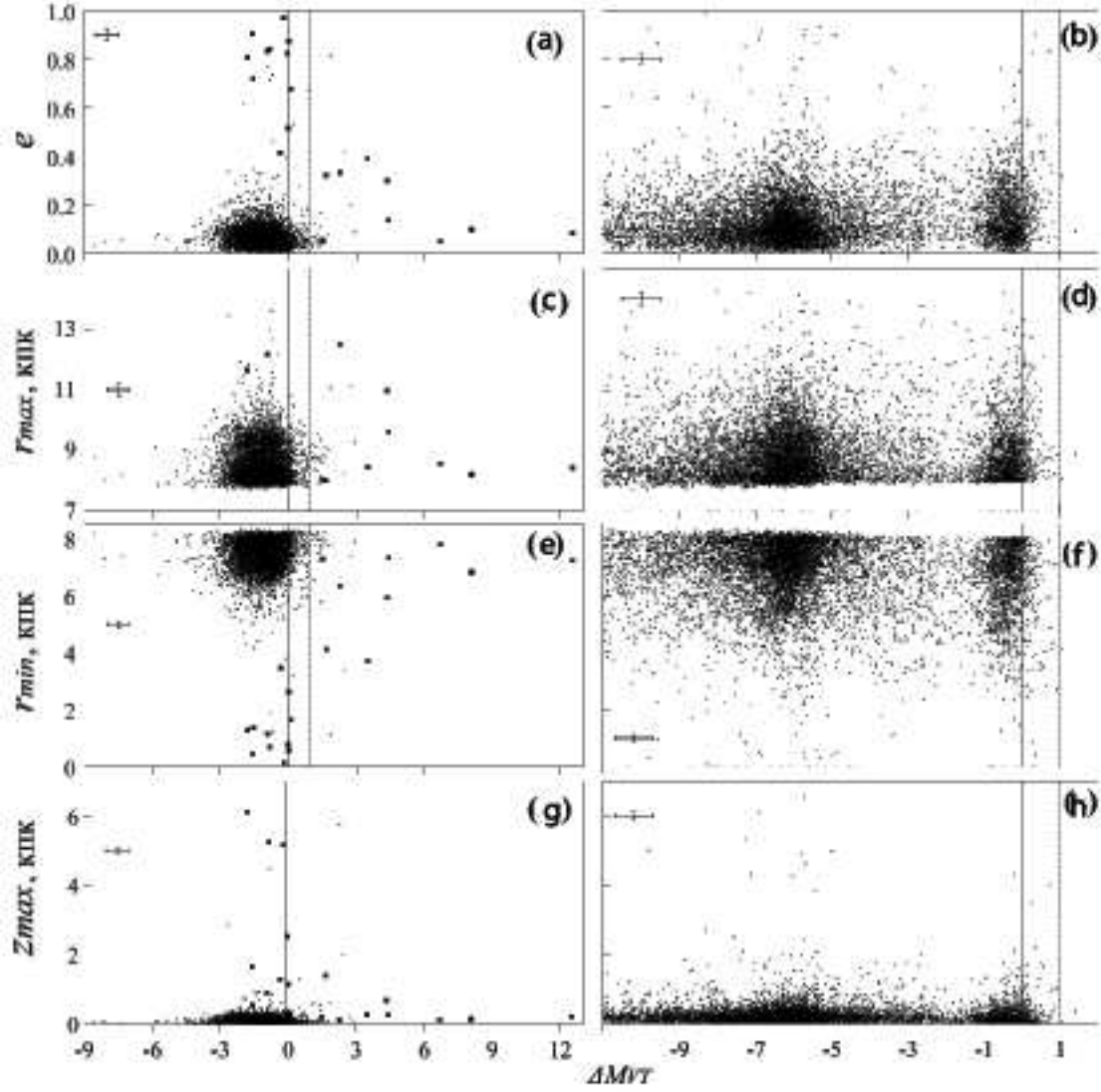


Figure 7: Positions of 5377 stars from the OA subsample and 9463 stars from the KM subsample on the “ $\Delta M_{V_T} - e$ ” (a) and (b), “ $\Delta M_{V_T} - r_{max}$ ” (c) and (d), “ $\Delta M_{V_T} - r_{min}$ ” (e) and (f), “ $\Delta M_{V_T} - Z_{max}$ ” (g) and (h) diagrams. The solid vertical straight line marks $\Delta M_{V_T} = 0^m$ and the dashed straight line marks $\Delta M_{V_T} = 1^M$, which corresponds to a 2σ error in calculating M_{V_T} . The crosses indicate typical errors for a star.

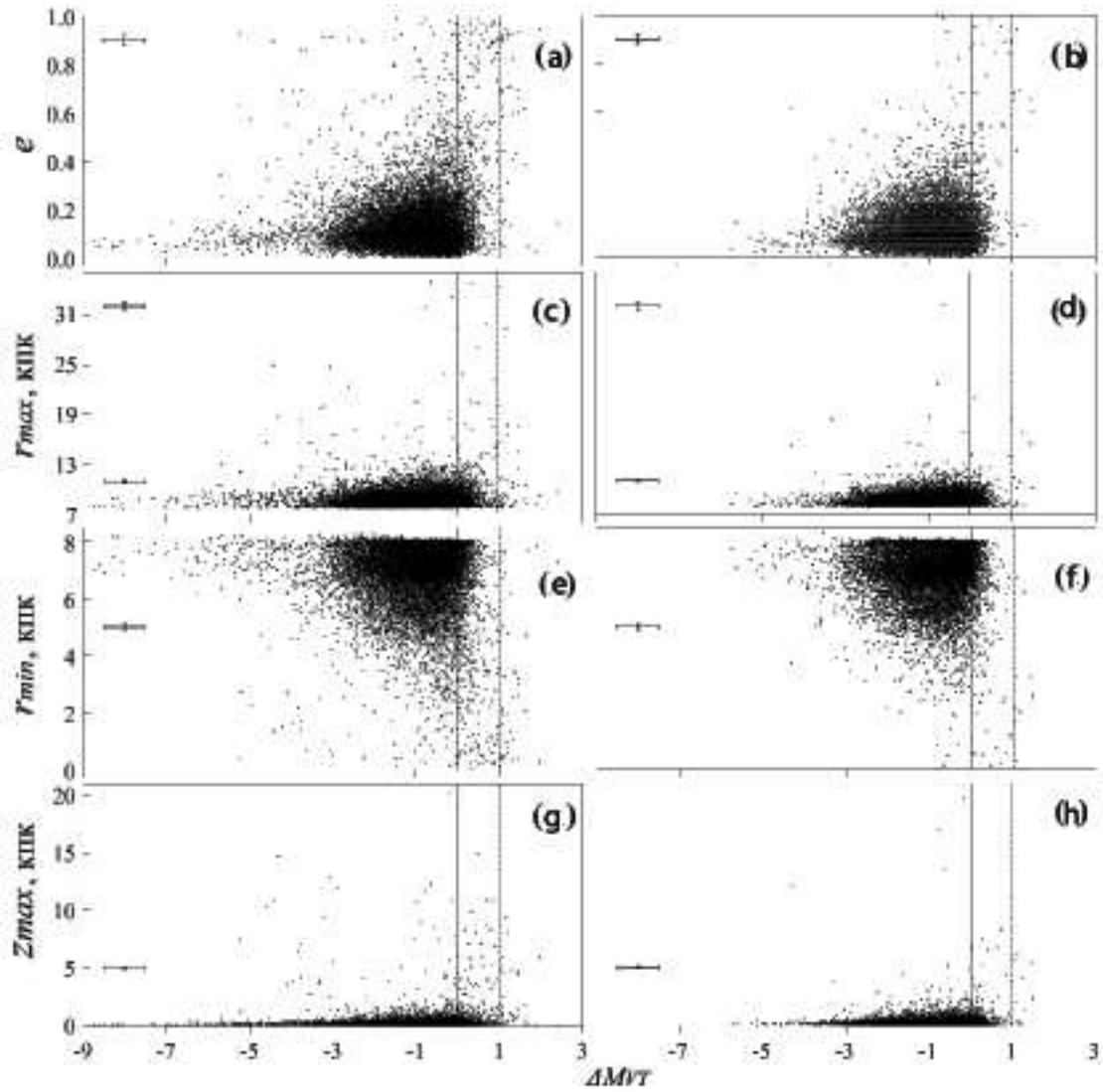


Figure 8: Same as Fig. 7 for 12 600 stars from the FG subsample and GCS stars from the FG subsample.